A Photopatternable Silicone for Biological Applications

Salil P. Desai,[†,‡] Brian M. Taff,[†,‡,§] and Joel Voldman*[,‡]

Department of Electrical Engineering and Computer Science, Massachusetts Institute of Technology, Cambridge, Massachusetts 02139, and Department of Systems Biology, Harvard Medical School, Boston, Massachusetts 02115

Received September 12, 2007. In Final Form: October 19, 2007

We show the application of a commercially available photopatternable silicone (PPS) that combines the advantageous features of both PDMS and SU-8 to address a critical bioMEMS materials deficiency. Using PPS, we demonstrate the ability to pattern free-standing mechanically isolated elastomeric structures on a silicon substrate: a feat that is challenging to accomplish using soft lithography-based fabrication. PPS readily integrates with many cell-based bioMEMS since it exhibits low autofluorescence and cells easily attach and proliferate on PPS-coated substrates. Because of its inherent photopatternable properties, PPS is compatible with standard microfabrication processes and easily aligns to complex featured substrates on a wafer scale. By leveraging PPS' unique properties, we demonstrate the design of a simple dielectrophoresis-based bioMEMS device for patterning mammalian cells. The key material properties and integration capabilities explored in this work should present new avenues for exploring silicone microstructures for the design and implementation of increasingly complex bioMEMS architectures.

Introduction

Polydimethylsiloxane (PDMS) has emerged as one of the most commonly used bioMEMS materials because it displays low autofluorescence, presents well-characterized biocompatibility,[1,2] and molds with reasonably high resolution.[3] PDMS devices are most commonly molded from photolithographically defined masters using either positive- or negative-tone photoresists, in a process termed soft lithography. Consequently, the geometry of PDMS structural features is defined by the resolution and fabrication constraints of the photoresist used when manufacturing the master. Moreover, PDMS or other elastomeric materials such as RTV (room temperature vulcanizing silicone rubber) molded using soft lithography suffer from several limitations:− (1) high aspect ratio structures are susceptible to mechanical collapse, (2) wafer-scale integration and micrometer-scale alignment with patterned substrates is challenging, and (3) free-standing, mechanically isolated microstructures are difficult to realize. Further, while PDMS films can be spun cast onto wafers, they are not easily directly patterned using conventional photolithographic techniques. Past work in developing photopatternable PDMS has involved adding photoinitiators to conventional PDMS (Sylgard 184) pre-polymers[4,5] or custom synthesis of polymers with inherent photopatterning capabilities and enhanced feature resolution.[6] None of these photopatternable PDMS formulations is commercially available. To avoid synthesizing photopatternable PDMS, SU-8 has been used as a photolithographically defined film to produce free-standing features in several bioMEMS applications.[7−9] While SU-8 is easily photopatterned, it is highly autofluorescent and thus poorly suited for the high-contrast fluorescence imaging that is critical to many bioMEMS applications. In our work, we demonstrate the use of a commercially available photopatternable silicone, PPS (WL-5150, Dow Corning Corporation) that combines several key advantages of both PDMS and SU-8. PPS obviates the need for custom synthesis, and its inherent photopatternability helps address some limitations associated with soft lithography-based methods. This material thereby presents new capabilities in the design and fabrication of biological microsystems.

PPS was originally developed for the electronics industry and has been used for several advanced packaging applications.[10−12] PPS chemistries are considered proprietary, and the exact chemical compositions are not freely available. In general, the chemical

* To whom correspondence should be addressed. Tel.: (617) 253-2094; fax: (617) 258-5846; e-mail: voldman@mit.edu.

† Both authors contributed equally to this work.

‡ Massachusetts Institute of Technology.

§ Harvard Medical School.

(1) Lee, J. N.; Jiang, X.; Ryan, D.; Whitesides, G. M. Compatibility of mammalian cells on surfaces of poly(dimethylsiloxane). *Langmuir* **2004**, *20* (26), 11684−11691.

(2) Peterson, S. L.; McDonald, A.; Gourley, P. L.; Sasaki, D. Y. Poly(dimethylsiloxane) thin films as biocompatible coatings for microfluidic devices: Cell culture and flow studies with glial cells. *J. Biomed. Mater. Res., Part A* **2005**, *72* (1), 10−18.

(3) Quake, S. R.; Scherer, A. From micro- to nanofabrication with soft materials. *Science (Washington, DC, U.S.)* **2000**, *290* (5496), 1536−1540.

(4) Choi, K. M.; Rogers, J. A. *Novel Chemical Approach to Achieve Advanced Soft Lithography by Developing New Stiffer, Photocurable PDMS Stamp Materials*, Nanoengineered Assemblies and Advanced Micro Nanosystems, San Francisco, CA, April 13−16, 2004; Materials Research Society: San Francisco, CA, 2004; pp 147−154.

(5) Bhagat, A. A. S.; Jothimuthu, P.; Papautsky, I. In *Photodefinable PDMS for Rapid Prototyping of Disposable Lab-on-a-Chip Systems*, Micro Total Analysis Systems 2006, Tokyo, Nov 5−9, 2006; Kitamori, T., Fujita, H., Hasebe, S., Eds.; Society for Chemistry and Micro-Nano Systems (CHEMINAS): Tokyo, Japan, 2006; pp 663−665.

(6) Choi, K. M.; Rogers, J. A. A photocurable poly(dimethylsiloxane) chemistry designed for soft lithographic molding and printing in the nanometer regime. *J. Am. Chem. Soc.* **2003**, *125* (14), 4060−4061.

(7) Jhanvi, H. D.; Yang, S.; Butler, P. J. Improved nanometer-scale particle tracking in optical microscopy using microfabricated fiduciary posts. *BioTechniques* **2007**, *42* (4), 437−440.

(8) Chronis, N.; Lee, L. P. Electrothermally activated SU-8 microgripper for single cell manipulation in solution. *J. Microelectromech. Syst.* **2005**, *14* (4), 857−63.

(9) Salazar, G. T. A.; Wang, Y.; Young, G.; Bachman, M.; Sims, C. E.; Li, G. P.; Allbritton, N. L. Micropallet arrays for the separation of single, adherent cells. *Anal. Chem.* **2007**, *79* (2), 682−687.

(10) Krassow, H.; Campabadal, F.; Lora-Tamayo, E. *Wafer Level Packaging of Silicon Pressure Sensors*, Transducers '99: 10th International Conference on Solid State Sensors and Actuators, Sendai, Japan, June 7−10, 1999; Elsevier: Amsterdam, 2000; pp 229−33.

(11) Vanden Bulcke, M.; Gonzalez, M.; Vandevelde, B.; Winters, C.; Beyne, E.; Larson, L.; Harkness, B. R.; Gardner, G.; Mohamed, M.; Sudbury-Holtschlag, J.; Meynen, H. *Introducing a Silicone under the Bump Configuration for Stress Relief in a Wafer Level Package*, Proceedings of the 5th Electronics Packaging Technology Conference (EPTC 2003), Singapore, Dec 10−12, 2003; IEEE: Singapore, 2003; pp 380−384.

(12) Meynen, H.; Bulcke, M. V.; Gonzalez, M.; Harkness, B.; Gardner, G.; Sudbury-Holtschlag, J.; Vandevelde, B.; Winters, C.; Beyne, E. *Ultra Low Stress and Low Temperature Patternable Silicone Materials for Applications within Microelectronics*, Materials for Advanced Metallization, Brussels, Belgium, March 7−10, 2004; Elsevier: Amsterdam, 2004; pp 212−218.

10.1021/la702827v CCC: $40.75
Published on Web 12/15/2007

composition of PPS is a silicone resin dissolved in a plasticizing matrix.[13] The ratio of solvent (typically mesitylene) added to this mixture facilitates spin coating and control of the final film thickness. UV exposure followed by thermal curing results in a cross-linking reaction of the silicone constituents that produces a three-dimensional network structure. The light-activated catalyst provides chemical cross-linking that is more thermally stable than that obtained using traditional epoxy-based cure chemistries and further allows for minimal shrinkage during cure.[13]

We believe that PPS' compatibility with standard microfabrication processing makes it an excellent candidate material for the design and fabrication of bioMEMS architectures. To this end, we characterize and demonstrate its relevance by presenting several inherent properties that demonstrate both its advantages and its disadvantages as a materials system for bioMEMS.

Results

Key Mechanical and Print Properties. To date, in the bioMEMS community, SU-8 negative photoresists are the dominant materials for polymeric feature fabrication. In our work, we evaluated the recently developed PPS chemistry developed by Dow Corning and compared some of its key properties to those of SU-8. In Figure 1, we compare patterns created using SU-8 and PPS. One important parameter in a structural material is the sidewall angle. While SU-8 offers re-entrant profiles of $\sim 94 \pm 2°$ ($n = 12$), PPS provides sidewall angles of $\sim 76 \pm 1°$ ($n = 8$) (Figure 1A,B). SU-8 is available in a variety of different solvent formulations that provide micrometer-scale pattern resolution across a range of tunable thicknesses. To assess the resolution of PPS in the context of SU-8 patterning capabilities, we used a standard resolution test target (USAF 1951) to photopattern features with both materials. As expected from its tapered sidewall profile, the resolution of our nominal 20 μm thick PPS test structures is reduced when compared to SU-8 structures of equivalent thickness. The ultimate resolution that we could repeatedly print was ~ 10 μm, as opposed to ~ 6 μm for SU-8.

One interesting and important feature of PPS is its robust adhesion to the substrate. In all cases, when we examined the smallest patterned PPS features, although they were ill-formed, they did remain firmly fastened to the substrate. In contrast, many small SU-8 features (line width ~ 5 μm) were missing entirely from the wafer, suggesting that they had suffered from poor adhesion. In subsequent probe tests, PPS structures stretched away from the substrate and even ripped prior to separation from the underlying wafer (data not shown). This behavior comes in stark contrast to similar SU-8 features, which completely detached from the wafer when subjected to comparable probing forces.

Free-Standing Microstructures. Free-standing mechanically isolated microstructures are challenging to produce using soft lithographic fabrication techniques. Prior attempts to create such structures have employed various specialized techniques where thin structured membranes were formed by either sandwiching poured PDMS between photolithographic masters[14] or carefully adjusting the pour height such that the tops of the masters protrude from the film.[15] In all of these implementations, a thin residual layer of PDMS remained affixed to the end fabricated substrate such that any patterned features were linked together by means of a common membrane backbone. To the best of our knowledge, physically isolated polymer microstructures patterned on a substrate have never been realized using molding techniques. In contrast, using PPS, it is possible to fabricate free-standing elastomeric microstructures (Figure 2). By patterning numerous types of cylindrical posts with square and circular top-down geometries, we readily reproduced structures with aspect ratios of 3:1 (measured as height/width).

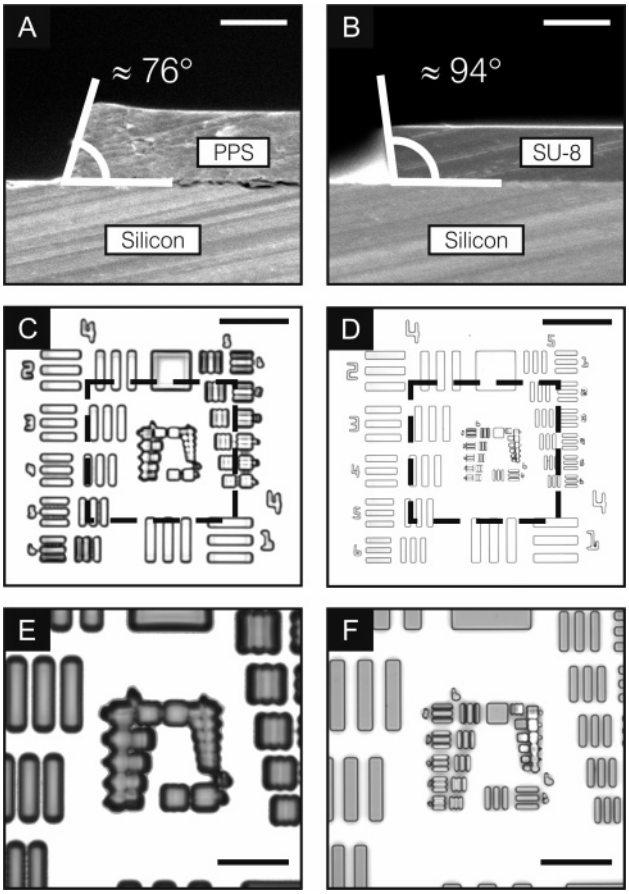

Figure 1. PPS sidewall angle and resolution. In panels A and B, we show scanning electron micrographs of sidewall angles formed using PPS and SU-8. Scale bars = 25 μm. In panels C and D, we provide bright-field microscopy images of the standard USAF 1951 resolution test pattern photopatterned in PPS and SU-8, respectively. Scale bars = 50 μm. Panel E and F examine the outlined regions in panels C and D, respectively, in closer detail. Scale bars = 25 μm.

Features exhibiting higher aspect ratios (>5:1) proved to be challenging to fabricate reliably using our current processing techniques. This complication likely reflects a fundamental limitation of the currently available PPS elastomer chemistry. Even with process optimization, we were unable to bring PPS aspect ratios to the level of SU-8. When attempting to fabricate high aspect ratio features in PPS, we commonly witnessed deformed posts that bent over and adhered to the substrate. Although the mechanisms are not entirely clear, the observed failure mode suggests that the patterned designs' mechanical properties are insufficient for self-support.

Biocompatibility. For widespread adoption of PPS as a material choice in the bioMEMS community, it is imperative to

(13) Harkness, B. R.; Gardner, G. B.; Alger, J. S.; Cummings, M. R.; Princing, J.; Lee, Y.; Meynen, H.; Gonzales, M.; Vandevelde, B.; Vanden Bulcke, M.; Winters, C.; Beyne, E. *Photopatternable Silicone Compositions for Electronic Packaging Applications*, Advances in Resist Technology and Processing XXI, Santa Clara, CA, Feb 23−24, 2004; SPIE−International Society of Optical Engineering: Santa Clara, CA, 2004; pp 517−524.

(14) Folch, A.; Jo, B.-H.; Hurtado, B.-H.; Beebe, D. J.; Hurtado, O.; Toner, M., Microfabricated elastomeric stencils for micropatterning cell cultures. *J. Biomed. Mater. Res.* **2000**, *52* (2), 346−353.

(15) Ostuni, E.; Kane, R.; Chen, C. S.; Ingber, D. E.; Whitesides, G. M., Patterning mammalian cells using elastomeric membranes. *Langmuir* **2000**, *16* (20), 7811−7819.

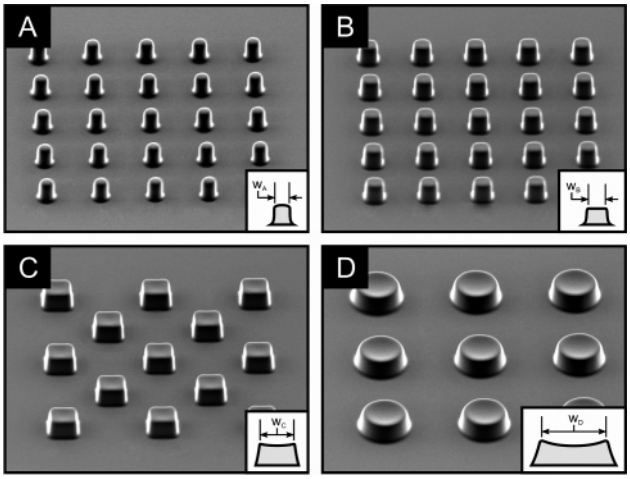

Figure 2. Free-standing PPS microstructures. SEM images of free-standing circular (A and D) and square (B and C) pillars patterned on a silicon substrate. In each inset, we provide a schematic image portraying the cross-sectional geometry of each feature ($w_A \approx 15$ μm, $w_B \approx 20$ μm, $w_C \approx 45$ μm, and $w_D \approx 80$ μm). Internal film stresses and feature edge geometries produce differing top surface profiles. Shapes with smaller footprints offer slightly convex tops, while features with larger footprints exhibit concave geometries.

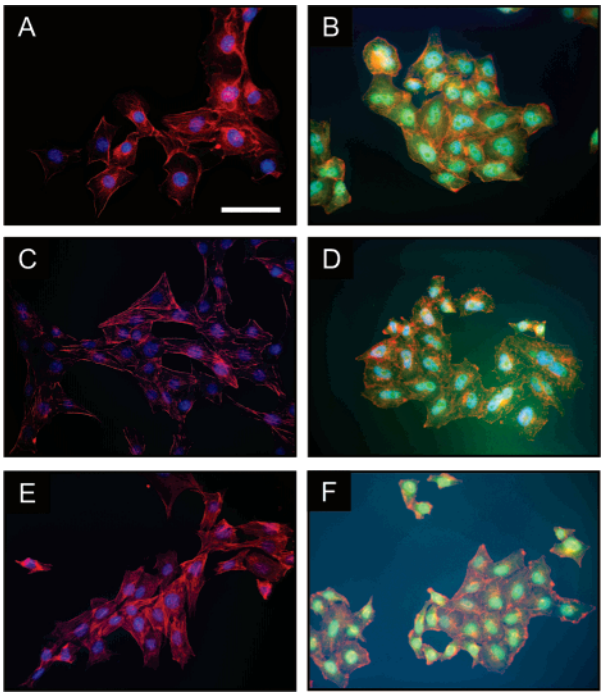

Figure 3. PPS biocompatibility. Fluorescence microscopy images showing NIH3T3 (A) and HeLa (B) cells grown on PPS for 4 days. To compare, panels C and D, respectively, offer images of 3T3 and HeLa cells plated and grown on TCPS dishes over the same duration. As an additional comparison, panels E and F, respectively, offer images of 3T3 and HeLa cells plated and grown on PDMS-coated substrates over the same duration. The images in panels A, C, and E represent merged actin (red) and DNA (blue) channel fluorescence, while those in panels B, D, and F additionally provide the constitutive EGFP expression (green) of the HeLa cell line. Scale bar = 50 μm.

characterize its biocompatibility. As a first step, we cultured both NIH 3T3 and HeLa cells, two lines commonly used in bioMEMS applications, on PPS-coated substrates for a span of 4 days (Figure 3A,B). At the end of the 4 day cultures, we stained the cells' actin and nuclei using standard immunofluorescence techniques. Cells cultured on PPS surfaces (Figure 3A,B) as well as those grown on comparative bioMEMS control surfaces—silicon nitride, SU-8, and PDMS (Figure 3E,F, and data not shown)—exhibited morphologies closely matching those typically seen in standard tissue culture polystyrene (TCPS) dishes (Figure 3C,D). This preliminary result shows that PPS does not result in any noticeable changes in cell morphology and furthermore does not significantly alter growth and proliferation of cells over 4 days. Because PPS' chemistry closely matches that of PDMS,[6] our results suggest that PPS may behave similarly to other biocompatible silicones.

Autofluorescence. Fluorescence-based assays are widely used in bioMEMS applications. Tracking, locating, and interrogating cells in microdevices commonly involves the use of various types of fluorescence imaging. It is thus imperative that the materials used in devices are not so autofluorescent as to impair image-based assays. To address this issue, we characterized the autofluorescence of PPS in the context of cell-based bioMEMS. HeLa cells with red, green, and blue fluorophores were imaged on TCPS and on silicon substrates coated with PPS, PDMS, SU-8, and silicon nitride (Figure 4A). The red, green, and blue fluorescence channels are representative of those used in most cell-based imaging. Exposure times for all the channels were chosen so as to enable high-contrast imaging on most of the substrates. Under these conditions, some of the images recorded on the SU-8 surfaces were saturated with background fluorescence. This saturation is caused by the higher autofluorescence of SU-8. To determine the intrinsic fluorescence of the different substrate coatings, we measured the autofluorescence of blank substrates (without cells) in the red, green, and blue fluorescence channels with the same exposure times used for cell imaging. Even though the exact same exposure times were used for obtaining images of different substrates with or without cells, it is not possible to make direct comparisons of the background fluorescence intensity in the images with cells (Figure 4A) to the quantitative measures of autofluorescence (Figure 4B). The images with cells (Figure 4A) provide a qualitative measure of the intrinsic fluorescence of the various substrates since the background fluorescence in these images could contain artifacts from cell staining procedures.

Fluorescence levels from PPS-coated substrates were similar to PDMS: ~1% greater in blue, 10% greater in green, and 4% greater in red (Figure 4B). SU-8-coated substrates exhibited much higher autofluorescence than PPS (Figure 4B), especially at shorter wavelengths (~2.5× brighter in red and ~15× brighter in blue and green). These results explain the saturated images obtained on SU-8 in Figure 4A. While it is certainly possible to optimize SU-8 exposure conditions to image cellular fluorescence (Figure 4C), the autofluorescence of SU-8 (Figure 4B) fundamentally decreases the contrast between sample and background, limiting the ability to perform sensitive fluorescence-based assays.[8]

Multilevel Alignment Fidelity. In contrast to standard master-molded PDMS, PPS enables wafer-scale feature alignment. Because it behaves as a standard negative photoresist, it is straightforward to position patterned PPS features onto underlying substrate registration marks with in-plane placement accuracies in the 2−3 μm range across 150 mm wafers (Figure 5A−C). This large-area alignment extends well beyond the typical capabilities of molded PDMS. Specifically, the flexible nature of molded PDMS slabs makes it challenging to align them to other patterned geometries.

Functional Device Operation. Finally, we wanted to demonstrate that the ability to align PPS to underlying features (in this case, metal) allowed for the creation of functional bioMEMS devices. We first fabricated a simple bioMEMS device (Figure

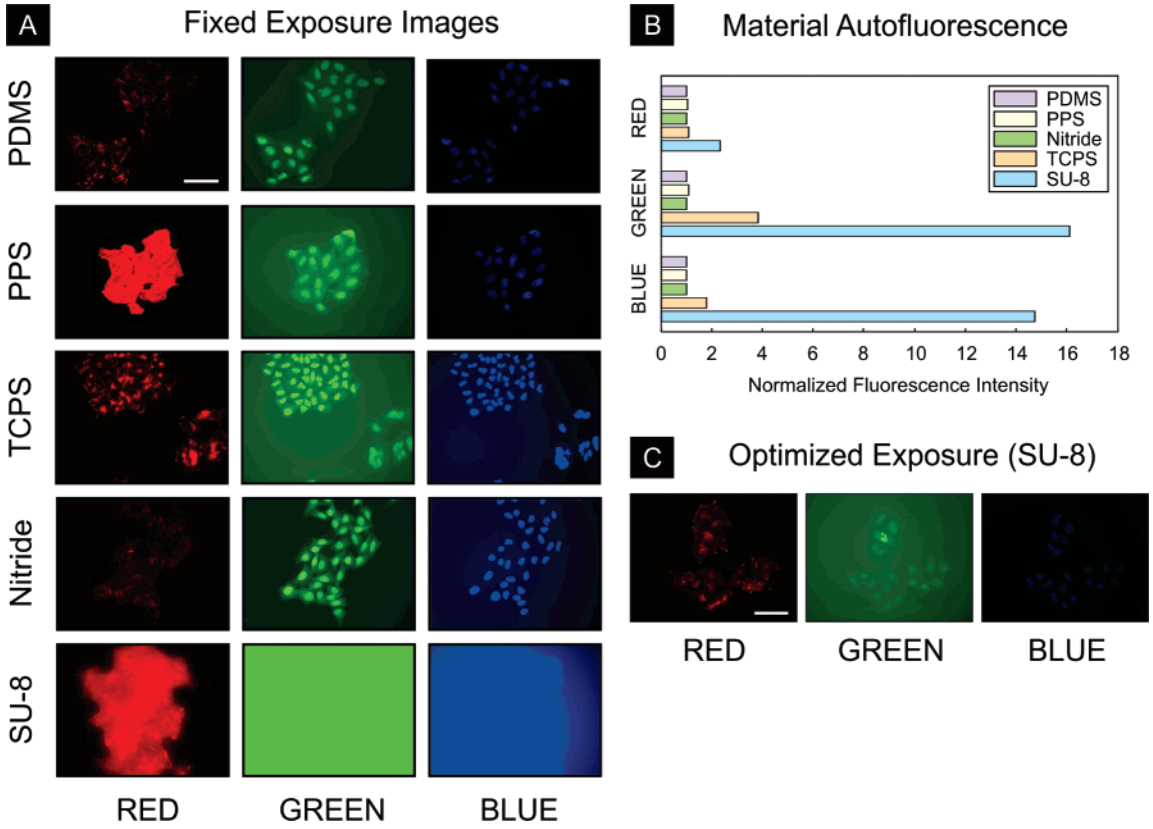

Figure 4. Autofluorescence. (A) Fluorescence images taken at fixed exposure times for red (750 ms), green (3000 ms), and blue (150 ms) channels of dual-stained EGFP + HeLa cells imaged on PDMS, PPS, silicon nitride, TCPS, and SU-8. Scale bar = 50 μm. (B) Quantitative comparison of fluorescence intensities of PDMS, PPS, nitride, TCPS, and SU-8 (normalized to PDMS), indicating high autofluorescence of SU-8 in green and blue channels, explaining the saturated images in panel A. Fluorescence imaging can be performed on SU-8 substrates by optimizing for exposure times. Representative images are shown in panel C. Scale bar = 50 μm.

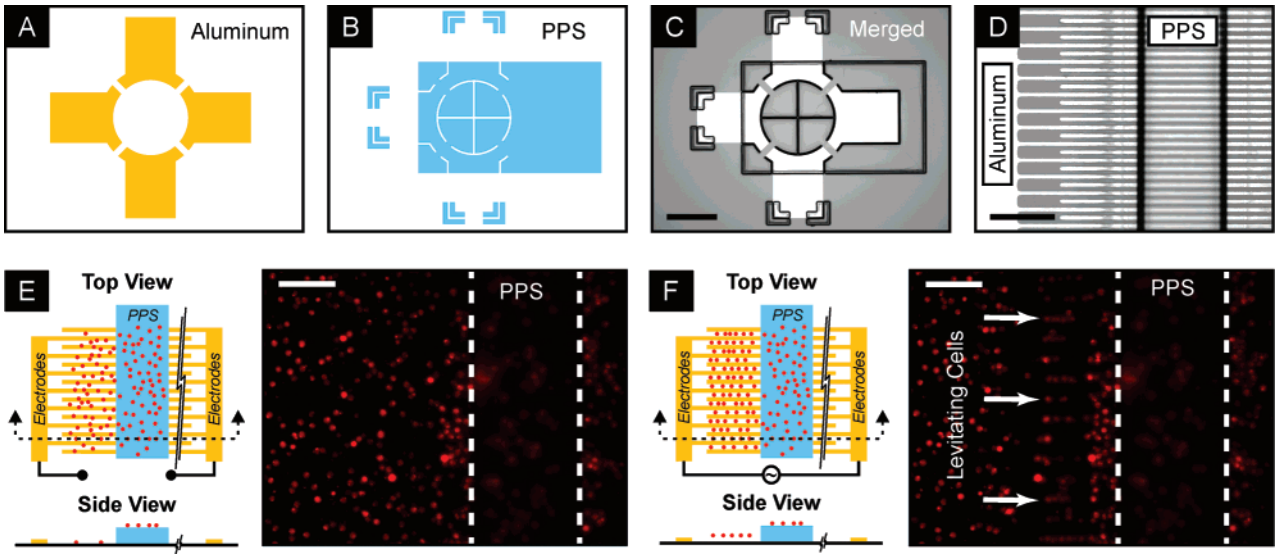

Figure 5. Alignment and cell patterning. A PPS structure was aligned to an aluminum metal layer as outlined schematically in panels A and B. Panel C presents a bright-field image of the resulting structure. Scale bar = 500 μm. Panel D shows a bright-field image detailing the top-down view of a simple dielectrophoretic cell manipulation structure, where a 20 μm tall PPS strip was aligned to an interdigitated aluminum electrode array positioned within a surrounding flow chamber. Scale bar = 200 μm. Panels E and F demonstrate the basic functionality of this device. Schematics show that when no voltage appears across the electrodes (orange), cells (red circles) initially settle randomly across the device surface (E). After electrode activation, cells respond to imposed negative DEP forces in select regions of the device, causing overlying cells to levitate and organize into bands (F). Both panel E and panel F show fluorescent images from actual devices operating with DsRed + BA/F3 cells. In panel E, cells that initially resided upon the patterned PPS strip (slightly out-of-focus due to their elevated height with respect to the substrate-affixed electrodes) were left in their original unorganized state. In panel F, arrows highlight a few of the organized levitating cell bands. Scale bars = 50 μm.

5D) that consisted of patterned strips of PPS aligned over a bank of underlying interdigitated electrodes. We then pipetted DsRed-expressing BA/F3 cells onto the devices and stimulated the on-chip electrodes using a 5 Vpp signal delivered at 500 kHz. As shown in Figure 5E, prior to voltage application, cells were randomly distributed across the chip surface. Applying voltages,

in turn, created negative dielectrophoretic (DEP) forces in regions of the device where uncovered electrodes were present. These DEP forces lifted stimulated cells vertically away from the interdigitated electrode edges. Subject to this stimulation, the cells organized into distinct levitating bands. Alternatively, the regions covered with PPS patterns left cells unaffected by DEP forces as the overlying PPS insulated the solution from on-chip electric fields (Figure 5F). The fact that DEP forces are created in the unmasked areas suggests that little or no PPS film remains in those regions; in highly conductive cell culture media, even nanometer-thick residual insulating films left on the device surface would be sufficient to eliminate the electric field in the solution (see Supporting Information).

Discussion

PPS was originally developed for the electronics packaging industry. To date, its major applications have included new approaches for flip-chip solder-bump designs[11,12] and wafer-scale pressure sensor enclosures.[10] It is commercially available in numerous solvent formulations and photopatterning resolutions. We chose a chemistry suitable for creating the micrometer-scale geometries typically found in many bioMEMS devices. In our work, we explored and leveraged PPS' properties integrating the material for the first time in devices designed for use with mammalian cells. Examining its capabilities and its limitations in the context of the demands imposed by biological microsystem applications sheds new light on its overall functionality and usability.

A primary feature of PPS is its low autofluorescence. With an autofluorescence level comparable to that of PDMS, this material provides a significant advantage over SU-8 for biological imaging (Figure 4). In microsystems where one wishes to perform fluorescence imaging, PPS offers significantly enhanced contrast over SU-8. This low autofluorescence is somewhat surprising since many photopatternable polymers (including SU-8) demand cationic activation of epoxy side chain groups and an associated cross-linking of shared aromatic hydrocarbon backbones.[16] Such aromatic constructs, with characteristically delocalized π-bond p-orbital overlap, permit a multitude of electron energy states that typically provide affiliated compounds with substantial, widely reported,[17−22] native autofluorescence characteristics. Thus, PPS' low autofluorescence was welcome and fundamental to our enthusiasm for the material.

We found the resolution of PPS to be moderate, primarily limited by its sidewall angle. SU-8, in contrast, patterns with much higher resolution (for equivalent thicknesses) due to its almost vertical re-entrant profile. The resolution of PDMS structures is determined by the master from which they are cast and can vary from tens of micrometers to the sub-micrometer regime. Since many bioMEMS devices only require moderate resolution, PPS offers wide applicability, although for small structures or those with near-vertical re-entrant sidewalls, PDMS or SU-8 are better choices.

Although the resolution of PPS is lower than that of SU-8 and PDMS, its ability to form mechanically isolated low-autofluorescent structures distinguishes it from these two materials. Specifically, SU-8 enables isolated highly fluorescent structures, while PDMS suits applications requiring contiguous, low-autofluorescent structures. The enhanced flexibility provided by PPS-based low-autofluorescent isolated features directly addresses many of the limitations in prior microsystems with image-dependent applications spanning from actin cortex studies[23] to single-cell analyses[9] and manipulation,[8] and even DNA microstructure analyses for advanced fluorescent in situ hybridization (FISH) assays.[24]

One potential limitation of PPS is the current upper bound for fabricated structure thicknesses. SU-8 and PDMS both provide the flexibility to form features that are greater than 100 μm in height using a single spun layer. In contrast, single layers of PPS currently enable feature heights of only $\sim$40 μm and lower. This characteristic is likely not intrinsic to the material but rather a limitation of the viscosities of available formulations. It may be possible to increase PPS layer thicknesses by varying the product formulation, although the likely continued presence of a 75° sidewall angle would ultimately limit the utility of thick (>100 μm) structures. While the 40 μm single-spin layer thickness limitation precludes the use of PPS for many structural applications, we believe that it still enables remarkable design flexibility serving a wide variety of uses. The material opens avenues for assembling fluid chambers where micropatterned PPS gaskets separate rigid top and bottom planes. This enhancement enables designs where pressure driven flow will not deform cross-sectional chamber geometries in high-throughput applications. Because PPS readily plasma bonds to glass, it avoids the additional process complexity needed for bonding of SU-8 gaskets to glass.[25] Thus, PPS, even in its current formulations, offers benefits for designing structures of moderate heights. In contrast, SU-8 and PDMS are likely better choices for applications requiring precisely formed tall structures.

PPS is processed as a conventional photoresist and thereby benefits from the alignment capabilities of photolithography. This functionality is similar to SU-8 but a significant advantage over PDMS, which requires alignment of a flexible substrate after separation from its master. In addition, PPS adheres to underlying metals, unlike PDMS, and in our hands offers better adhesion to the substrate than SU-8. This flexibility offers a means to form multilayer structures that combine metals, dielectrics, and low-autofluorescent structural layers. We demonstrate one such device in Figure 5. Essentially, any microsytems-based design that utilizes on-chip electrodes presents a potential application space for this photopatterned polymer system. A wide variety of bioMEMS electroporation and electrofusion

(16) Shaw, J. M.; Gelorme, J. D.; Labianca, N. C.; Conley, W. E.; Holmes, S. J., Negative photoresists for optical lithography. *IBM J. Res. Dev.* **1997**, *41* (1−2), 81−94.

(17) Gauthier, T. D.; Shane, E. C.; Guerin, W. F.; Seitz, W. R.; Grant, C. L. Fluorescence quenching method for determining equilibrium constants for polycyclic aromatic hydrocarbons binding to dissolved humic materials. *Environ. Sci. Technol.* **1986**, *20* (11), 1162−1166.

(18) Hasegawa, M.; Kochi, M.; Mita, I.; Yokota, R. Molecular aggregation and fluorescence spectra of aromatic polyimides. *Eur. Polym. J.* **1989**, *25* (4), 349−354.

(19) Nohta, H.; Yukizawau, T.; Ohkura, Y.; Yoshimura, M. Aromatic glycinonitriles and methylamines as pre-column fluorescence derivatization reagents for catecholamines. *Anal. Chim. Acta* **1997**, *344* (3), 233−240.

(20) Backhus, D. A.; Gschwend, P. M. Fluorescent polycyclic aromatic hydrocarbons as probes for studying the impact of colloids on pollutant transport in groundwater. *Environ. Sci. Technol.* **1990**, *24* (8), 1214−1223.

(21) Nie, S.; Dadoo, R.; Zare, R. N. Ultrasensitive fluorescence detection of polycyclic aromatic hydrocarbons in capillary electrophoresis. *Anal. Chem.* **1993**, *65* (24), 3571−3575.

(22) Pinto, C. G.; Pavon, J. L. P.; Cordero, B. M. Cloud point preconcentration and high-performance liquid chromatographic determination of polycyclic aromatic hydrocarbons with fluorescence detection. *Anal. Chem.* **1994**, *66* (6), 874−881.

(23) Roos, W. H.; Roth, A.; Konle, J.; Presting, H.; Sackmann, E.; Spatz, J. P. Freely suspended actin cortex models on arrays of microfabricated pillars. *ChemPhysChem* **2003**, *4* (8), 872−877.

(24) Terao, K.; Kabata, H.; Washizu, M. Extending chromosomal DNA in microstructures using electroosmotic flow. *J. Phys.: Condens. Matter* **2006**, *18* (18), 653−663.

(25) Jackman, R. J.; Floyd, T. M.; Ghodssi, R.; Schmidt, M. A.; Jensen, K. F. Microfluidic systems with on-line UV detection fabricated in photodefinable epoxy. *J. Micromech. Microeng.* **2001**, *11* (3), 263−269.

devices[26] is thus well-positioned to benefit from the integration capabilities offered by PPS. In some electrokinetic flow devices,[27] external power source demands could be reduced by positioning electrodes on-chip. Elaborate microscaffold architectures for 3-D cell perfusion,[28] stand-alone flow-through chip designs,[29] neuronal patterning structures,[30] and even patch clamp applications[31] could benefit from enhanced fluorescence imaging capabilities through PPS-based structures. If low autofluorescence is not mandated, SU-8 may better suit multilevel applications, due to its maturity, resolution, and thickness range, but PPS does present a compelling alternative for designs involving fluorescence assays.

One key application for SU-8 and PDMS is relief casting, where SU-8 serves as a mold for casting PDMS. While it may prove to be feasible to silanize PPS patterns and subsequently form relief-based architectures in PDMS, PPS is better suited for other applications. Although PPS' non-re-entrant sidewalls could ease PDMS mold removal, the thicknesses and resolutions achievable in the template geometries would generally underperform equivalent designs formed using SU-8. While rapid PDMS prototyping leverages repeated castings from a single master, PPS features cannot be recreated without returning to the cleanroom.

In this study, we have taken preliminary steps to characterize the relevance of PPS as a biomaterial. Admittedly, the notion of biocompatibility is far too general a concept to examine exhaustively.[2,32−36] Proving that a given material presents no biological effects for all applications is impossible. Our initial examinations do, however, suggest that PPS holds promise as a biomaterial. In the context of polymer-based biological materials, researchers have significantly more experience with both SU-8 and PDMS. PDMS has seen routine use with cells for more than 20 years.[37,38] SU-8 has also been used with cells, even primary cells,[28,39] although researchers often perform a solvent extraction step beforehand to aid biocompatibility.[40] The dearth of historical familiarity with PPS as a biomaterial thus presents a notable barrier to its widespread adoption.

In summary, the properties of PPS position it for a suite of applications not currently covered by SU-8 and PDMS. PPS will admittedly require further support and characterization before widespread adoption is likely. As an effort to fill this information void, we have presented here the key properties and functionalities associated with PPS in the context of the material's applicability to biological microsystems. Through continued research, PPS may become more commonplace in designs and offset a number of limitations associated with the current suite of materials for bioMEMS device fabrication.

Conclusion

We have examined some of the functional properties of a newly available commercial photopatternable silicone from the perspective of biological microsystems applications. PPS provides a unique combination of properties currently lacking in any one polymer commonly used for bioMEMS device architectures. It can readily form free-standing features on wafer-scale substrates, and its low autofluorescence provides a means to construct substrate-attached polymer structures suitable for high-contrast fluorescence-based imaging. Because the non-exposed regions in PPS patterns are largely residue-free, it ideally suits applications where substrate electrode geometries must remain uncovered. As its pattern formation leverages standard photoresist processing, aligning the material with pre-patterned features on a substrate is straightforward. Finally, the lack of any obvious morphological changes in cell cultures grown in direct contact with PPS holds promise for its incorporation in biological microsystems. With its unique set of properties, we believe that PPS is poised to join SU-8 and PDMS as a widely used bioMEMS material.

Materials and Methods

Surface Preparation for Cell Culture. We cultured cells on the following surfaces: (1) SU-8 2015 (Microchem), (2) Sylgard 184 PDMS (Dow Corning), (3) PPS (Dow Corning), (4) silicon nitride, and (5) Nunclon Delta 35 mm TCPS dishes (Nunc). For SU-8, PDMS, and PPS, we coated each film onto an underlying 100 mm silicon wafer targeting nominal cured thicknesses of 20 μm (confirmed by DEKTAK profilometry readings—data not shown). To prepare wafers, we cleaned them in an oxygen plasma for 7 min followed by a 10 min dehydration bake at 250 °C. When coating SU-8, we followed standard processing recipes except that we slowly ramped temperatures during bakes. We prepared the PDMS films using a 10:1 base/hardener mixture that we spun onto our wafers and then cured for 15 min at 100 °C. For the PPS coatings, we spread the film for 10 s at 500 rpm followed by 30 s at 2100 rpm. We then baked the films on a hotplate (2 min at 120 °C), flood-exposed them at 10 mJ/cm^2 (i-Line) using a mask aligner, and post-baked them (3 min at 150 °C on a hotplate). We developed the samples for 6 min in mesitylene (tri-methylbenzene, Sigma Aldrich) and cured them at 150 °C for 2 h. For our nitride surfaces, we used plasma enhanced chemical vapor depostion (PECVD) to deposit a 250 Å thick nitride film on a 150 mm silicon wafer. After die saw separation, we cleaned the chips in ethanol. On the day prior to cell seeding, we soaked the chips and TCPS dishes in deionized water for 12−16 h. This procedure adhered to those previously described,[40] which aimed to leach out any potential remnant solvents in the culture surfaces.

(26) Fox, M. B.; Esveld, D. C.; Valero, A.; Luttge, R.; Mastwijk, H. C.; Bartels, P. V.; Van Den Berg, A.; Boom, R. M. Electroporation of cells in microfluidic devices: A review. *Anal. Bioanal. Chem.* **2006**, *385* (3), 474−485.

(27) Skulan, A. J.; Barrett, L. M.; Singh, A. K.; Cummings, E. B.; Fiechtner, G. J. Fabrication and analysis of spatially uniform field electrokinetic flow devices: Theory and experiment. *Anal. Chem.* **2005**, *77* (21), 6790−6797.

(28) Rowe, L.; Almasri, M.; Lee, K.; Fogleman, N.; Brewer, G. J.; Nam, Y.; Wheeler, B. C.; Vukasinovic, J.; Glezer, A.; Frazier, A. B. Active 3-D microscaffold system with fluid perfusion for culturing in vitro neuronal networks. *Lab Chip* **2007**, *7* (4), 475−482.

(29) Jenke, M. G.; Schreiter, C.; Kim, G. M.; Vogel, H.; Brugger, J. Micropositioning and microscopic observation of individual picoliter-sized containers within SU-8 microchannels. *Microfluidics Nanofluidics* **2007**, *3* (2), 189−194.

(30) Wu, Z.-Z.; Zhao, Y.; Kisaalita, W. S. Interfacing SH-SY5Y human neuroblastoma cells with SU-8 microstructures. *Colloids Surf., B* **2006**, *52* (1), 14−21.

(31) Wilk, S. J.; Goryll, M.; Petrossian, L.; Laws, G. M.; Goodnick, S. M.; Thornton, T. J.; Saraniti, M.; Tang, J. M.; Eisenberg, R. S. *Microfabricated Silicon Apertures for Ion Channel Measurement*, 2005 NSTI Nanotechnology Conference and Trade Show, NSTI Nanotech 2005, Anaheim, CA, May 8−12, 2005; Nano Science and Technology Institute: Anaheim, CA, 2005; pp 504−507.

(32) Belanger, M.-C.; Marois, Y. Hemocompatibility, biocompatibility, inflammatory and in vivo studies of primary reference materials low-density polyethylene and polydimethylsiloxane: A review. *J. Biomed. Mater. Res.* **2001**, *58* (5), 467−477.

(33) Kotzar, G.; Freas, M.; Abel, P.; Fleischman, A.; Roy, S.; Zorman, C.; Moran, J. M.; Melzak, J. Evaluation of MEMS materials of construction for implantable medical devices. *Biomaterials* **2002**, *23* (13), 2737−2750.

(34) Tang, L.; Sheu, M.-S.; Chu, T.; Huang, Y. H. Anti-inflammatory properties of triblock siloxane copolymer-blended materials. *Biomaterials* **1999**, *20* (15), 1365−1370.

(35) Voskerician, G.; Shive, M. S.; Shawgo, R. S.; Von Recum, H.; Anderson, J. M.; Cima, M. J.; Langer, R. Biocompatibility and biofouling of MEMS drug delivery devices. *Biomaterials* **2003**, *24* (11), 1959−1967.

(36) Weisenberg, B. A.; Mooradian, D. L. Hemocompatibility of materials used in microelectromechanical systems: Platelet adhesion and morphology in vitro. *J. Biomed. Mater. Res.* **2002**, *60* (2), 283−291.

(37) Lindon, J. N.; Collins, R. E.; Coe, N. P.; Jagoda, A.; Brier-Russell, D.; Merrill, E. W.; Salzman, E. W. In vivo assessment in sheep of thromboresistant materials by determination of platelet survival. *Circ. Res.* **1980**, *46* (1), 84−90.

(38) Predecki, P.; Life, L.; Newman, M. M. Prevention of platelet adhesion to porous surfaces. *J. Biomed. Mater. Res.* **1980**, *14* (4), 405−415.

(39) Fissell, W. H.; Manley, S.; Westover, A.; Humes, H. D.; Fleischman, A. J.; Roy, S. Differentiated growth of human renal tubule cells on thin film and nanostructured materials. *ASAIO J.* **2006**, *52* (3), 221−227.

(40) Albrecht, D. R.; Liu Tsang, V.; Sah, R. L.; Bhatia, S. N. Photo- and electropatterning of hydrogel-encapsulated living cell arrays. *Lab Chip* **2005**, *5* (1), 111−118.

Plasmids. The DsRed T4 plasmid has been described previously[41] and was a gift from Susan Lindquist (Whitehead Institute, Cambridge, MA). Plasmids were amplified using chemically competent *Escherichia coli* strains (DH5α, Invitrogen). Plasmids were purified using a standard plasmid purification kit (Midiprep, Qiagen) from cultures grown in Luria broth overnight (standard *E. coli* culture protocols were used). Plasmid purity and concentration were subsequently assessed using a spectrophotometer (ND-1000, NanoDrop Technologies).

Cell Culture and Transfection. NIH 3T3 fibroblasts were purchased from ATCC and cultured as previously described.[42] EGFP + HeLa human carcinoma cells were a gift from Sangeeta Bhatia (MIT, Cambridge, MA). BA/F3 mouse pro B cells and WeHi-3B myelomonocytic leukemia cells were provided by Susan Lindquist (Whitehead Institute). B cells were cultured in RPMI medium supplemented with 10% (vol/vol) fetal bovine serum (FBS), 10% (vol/vol) WeHi-3B conditioned medium as a source of murine IL-3, 2% (vol/vol) L-glutamine taken from 200 mM stock (Gibco), 100 units/mL penicillin (Gibco), and 100 μg/mL streptomycin (Gibco). WeHi-3B leukemia cells were cultured in Iscove's modified Dulbecco's medium (IMDM) supplemented with 10% FBS, 2 mM l-glutamine, and 25 μM mercaptoethanol. WeHi-3B conditioned media were prepared as previously described.[43] BA/F3 cells were transfected using electroporation protocol X-01 (Amaxa Nucleofection) and subsequently underwent antibiotic selection in 1 mg/mL G-418 (Geneticin, Invitrogen) supplemented media for 4 weeks. Stably transfected cells were then sorted for the brightest clones using flow cytometry (Mo-Flo, Center for Cancer Research Flow Cytometry Core, MIT).

Cell Growth and Staining for Fluorescence-Based Imaging. Surface-coated chips and 35 mm TCPS dishes were first prepared as described previously. Subsequently, all surfaces (surface-coated chips and TCPS dishes) were plasma oxidized for 1 min, soaked in 80% ethanol for ~10 min, and dried under nitrogen. We then aseptically transferred individual surface-coated chips to separate wells in a 6-well plate ($n = 2$ for each chip type) and seeded all our surfaces with either NIH3T3 or HeLa cells using 2 mL of media/well at 1×10^4 cells/mL. We grew cultures for 4 days. On day 4, we fixed and permeabilized the cells and then stained for actin (rhodamine phalloidin R415, Invitrogen) and DNA (Hoechst 33258, pentahydrate, Invitrogen) using standard protocols. All PBS washes used $MgCl_2$- and $CaCl_2$-supplemented PBS to minimize cell detachment. We used 1% BSA throughout to minimize nonspecific staining. We first stained actin and then DNA, and in preparation for imaging, we mounted coverslips using a Flouromount G (Invitrogen) preservative.

Light Microscopy. A silicon die with PPS and SU-8 resolution targets was imaged using an AxioImager microscope (Carl Zeiss MicroImaging). Images were taken using 20× (0.5 NA) and 40× (0.75 NA) LD epiplan objectives (Carl Zeiss MicroImaging). All bright-field images were captured at 8 bit resolution using a cooled camera (LA Vision). Fixed cells were imaged in epifluorescence mode. Fluorescence illumination was provided by an XCite 100 (EXFO Life Sciences and Industrial Division) illumination source. EGFP (Set 38, Carl Zeiss MicroImaging), TRITC, and DAPI filter sets (31000 and 31002, Chroma Technology) were used for imaging constitutive EGFP expression, rhodamine phalloidin, and Hoechst nuclear stains, respectively. Fluorescence images were acquired with 12 bit resolution. To assess background fluorescence, silicon die coated with PPS, SU-8, PDMS and silicon nitride along with a 35 mm TCPS dish were imaged using epifluorescence microscopy and a 20× (0.5 NA) objective. Care was taken to ensure that all images were recorded with identical acquisition parameters (exposure time, camera gain, and microscope aperture settings).

Scanning Electron Microscopy. An individual die was cleaned with acetone and isopropyl alcohol and subsequently dried with nitrogen. The die was then sputtered coated with ~50 Å layer of gold in an argon plasma. The die was then mounted on standard flat mounts or angle mounts for imaging. Images were acquired at 5 kV acceleration and magnifications ranging from 250× to 400×.

Image Processing. Images were post-processed using MATLAB. Autofluorescence of uniformly coated substrates was determined by taking the average intensity of the entire fluorescence image for each fluorescence channel. Sidewall angles were assessed by analyzing SEM images with AutoCAD (Autodesk) and were measured from within patterned features using the wafer surface as a reference.

Aligned Electrode and PPS Device Fabrication. We fabricated our aligned electrode PPS devices on silicon substrates. We first grew a 1.5 μm thick silicon dioxide substrate isolation layer using wet thermal oxidation. We then sputter deposited a 5000 Å thick aluminum layer onto the wafers and etched electrodes using BCl_3− and Cl_2−plasma enhanced chemistries. We then deposited and patterned an aligned PPS layer (as stated previously). Because PPS spun films are exceptionally tacky, even after prebake steps, we placed cellophane (0.001 in. thick) rings around the perimeter of each wafer prior to soft contact mode exposure on a mask aligner. This ring of cellophane prevented direct contact between the wafer and the mask, eliminating failures due to mask−wafer adhesion. We protected the wafer surfaces using a standard positive photoresist and then separated chips with a die saw.

Chip Packaging. For our PPS electrode devices, we packaged individual chips by mounting them on glass slides using double-sided tape. We then affixed the slides to a standard upright microscope stage insert. We used laser-cut PDMS gaskets (250 μm thick, Bisco Silicones Inc.) around the active chip areas to form flow chambers. We then filled the chambers with cell suspensions and capped them with coverslips. We made electrical connections to the on-chip electrodes using alligator clips and delivered signals using an arbitrary waveform generator (Agilent 33250A).

Acknowledgment. We thank Alice Chen (from Sangeeta Bhatia's lab) and Sara Cullinan (from Susan Lindquist's lab) for providing us with cell lines, Luke Whitesell (from Susan Lindquist's lab) for help in plasmid preparation, and Prakash Rao (from Harvey Lodish's lab) and Calvin Jan (from David Bartel's lab) for assistance with transfection. We thank Herman Meynen for helpful technical discussions regarding PPS processing, Scott Manalis and the Media Laboratory at MIT for laser cutter facilities access, and Nicky Watson of the W. M. Keck Foundation at the Whitehead Institute for SEM assistance. Michael Vahey provided valuable feedback pertinent to electrical modeling of residual on-chip PPS films. This work was supported in part by the NIH (RR199652 and EB005753), the Singapore−MIT Alliance, and NSF Graduate Fellowship funding.

Supporting Information Available: Spin curve data, an examination of the electrical impact caused by residual PPS films, and detailed explanations of several processing techniques that proved pivotal for viable fabrication. This material is available free of charge via the Internet at http://pubs.acs.org.

LA702827V

(41) Bevis, B. J.; Glick, B. S. Rapidly maturing variants of the Discosoma red fluorescent protein (DsRed). *Nat. Biotechnol.* **2002**, *20* (1), 83−87.

(42) Kim, L.; Vahey, M. D.; Lee, H.-Y.; Voldman, J. Microfluidic arrays for logarithmically perfused embryonic stem cell culture. *Lab Chip* **2006**, *6* (3), 394−406.

(43) Ihle, J. N.; Keller, J.; Henderson, L.; Klein, F.; Palaszynski, E. Procedures for the purification of interleukin 3 to homogeneity. *J. Immunol.* **1982**, *129* (6), 2431−2436.